Int. J. Mech. Sci. Vol. 22, pp. 339–354
Pergamon Press Ltd., 1980. Printed in Great Britain

SURFACE INSTABILITIES ON STATICALLY STRAINED PLASTIC SOLIDS

J. W. HUTCHINSON
Division of Applied Sciences, Harvard University, Cambridge, MA 02138, U.S.A.

and

V. TVERGAARD
Department of Solid Mechanics, Technical University of Denmark, Lyngby, Denmark

(*Received* 25 *September* 1979; *in revised form* 12 *December* 1979)

Summary—An exploratory study is carried out of various aspects of the development of instabilities of traction-free surfaces of statically strained, rate-independent elastic–plastic solids. Existence of surface instabilities as predicted by either a bifurcation analysis or a quasi-static, imperfection-growth analysis, is found to be strongly dependent on the type of constitutive law assumed. In most instances no instabilities are found using the standard plastic flow law based on a smooth yield surface and isotropic hardening. Instabilities are predicted when a finite strain deformation theory is assumed. These are documented for a full range of proportional overall straining histories using a bifurcation analysis. A finite element analysis employing a corner theory of plasticity is used to study the non-linear growth of the instabilities starting from small initial surface undulations for the case of plane strain deformation. Some experimental observations of surface irregularities which may be due to surface instabilities are reported and discussed.

NOTATION

a_0	initial depth of cell (Fig. 5)
C_{ijkl}	instantaneous plastic compliance tensor (3·9)
E, E_t, E_s	Young's modulus, tangent modulus and secant modulus
f	specifies non-linear range at vertex (3·12)
g	hydrostatic part of the stress-rate (2·2)
k, k_2, k_3	were numbers in eigenmode (2·12–13)
l_0, l	initial and current half-wavelength (Fig. 5)
L_{ijkl}	instantaneous moduli
M_{ijkl}	elastic compliance tensor (3·9)
N	power hardening index
s_{ij}	deviator stress tensor
T_i	nominal traction vector
u_i	current displacements
v_i	velocity components of the eigenmode(2·12)
x_i	Cartesian coordinates
X	parameter increasing with strain level (2·1)
z	complex parameter in (A4)
α	angle defining fixed strain ratio (2.1)
β	angle defined by (A9)
δ_0, δ	initial and current wave height (Fig. 5)
δ_{ij}	Kronecker's delta
$\eta_{\alpha\beta}$	Lagrangian strain tensor (3.2)
θ	angular measure of stress-rate direction (3.11)
$\theta_0, \theta_c, \theta_n$	angles defining vertex on yield surface
ϵ_a	overall strain in x_2-direction (3.8)
ϵ_i	principal logarithmic strains
ϵ_0	yield strain
$\dot{\epsilon}_{ij}$	Eulerian strain-rate tensor
μ, μ^*	instantaneous shearing moduli (2.15)
σ_e	effective Mises stress
σ_i	true principal stresses
σ_0	yield stress
$\overset{*}{\sigma}_{ij}$	Jaumann co-rotational rate of the Cauchy stress tensor
$\tau^{\alpha\beta}$	contravariant components of Kirchhoff stress tensor
ϕ	angle defined by (A12)
Ω	angle defined by (2.13)

1. INTRODUCTION

The possibility that a plane, tractionless surface of a homogeneously strained solid loses flatness and develops surface undulations, or waves, was noted by Biot[1] in his study of the plane strain deformation of non-linearly elastic solids. His bifurcation analysis of the static deformation of a semi-infinite half-space reveals that the onset of surface modes occurs at a critical stress, or strain, which depends on the properties of the solid. Since there are no physical length quantities in the continuum formulation of the problem, the scale, or wavelength, of the surface mode is undetermined and may be arbitrarily short or long. The modes decay exponentially beneath the surface with a wavelength which is of the same order as the surface variation. Similar surface modes have been found in other plane strain studies by Sawyers[2] for non-linear elastic solids and by Hill and Hutchinson[3] and Young[4] for a wider range of solids, including elastic–plastic solids.

In this paper we pursue the subject further by using a bifurcation analysis to determine conditions for the onset of surface instabilities under more general combinations of homogeneous straining. A finite element method is used to study the non-linear growth of the surface instabilities, starting from an initial slight waviness of the surface, under conditions of plane strain. It will be noted that the existence of such instabilities depends strongly on the type of plasticity theory employed. Surface instabilities are excluded, except possibly at very large strains, in a solid characterized by a smooth yield surface and isotropic hardening. They do occur at moderately large strains in a solid characterized by a deformation, or corner, theory of plasticity.

Observations of surface irregularities due to straining will be reported and discussed. We will also speculate about the possible role of surface instabilities in the development of surface roughness.

2. BIFURCATION ANALYSIS OF SURFACE INSTABILITIES ON A HALF-SPACE

Let the undeformed semi-infinite half-space occupy the region $x_1 \le 0$ where x_i $(i = 1, 3)$ are set of fixed Cartesian axes. The material of the half-space is taken to be an incompressible, rate-independent solid which is initially isotropic, or at least orthotropic with respect to the x_i axes.

The fundamental straining history from which bifurcation occurs is prescribed to be a history of uniform proportional straining with principal axes x_i. With ϵ_i as the principal logarithmic strains, the fundamental history is prescribed by

$$\epsilon_2 = X\cos\alpha, \quad \epsilon_3 = X\sin\alpha, \quad \epsilon_1 = -\epsilon_2 - \epsilon_3 \tag{2.1}$$

where α is fixed and X is increased monotonically from zero. The principal axes of stress are also the x_i-axes for the fundamental solution and the true principal stresses are denoted by σ_i with $\sigma_1 = 0$ since the surface is traction-free. Without loss in generality, the free surface in the deformed fundamental state is taken coincident with $x_1 = 0$.

In the fundamental state, we consider incrementally linear behaviour in the form

$$\overset{*}{\sigma}_{ij} = L_{ijkl}\dot{\epsilon}_{kl} + g\delta_{ij} \quad (\dot{\epsilon}_{pp} = 0) \tag{2.2}$$

where $\overset{*}{\sigma}_{ij}$ is the Jaumann co-rotational rate of the Cauchy stress, $\dot{\epsilon}_{ij}$ is the Eulerian strain-rate and δ_{ij} is the Kronecker delta. Incompressibility requires $\dot{\epsilon}_{pp} = 0$ and g is the hydrostatic part of the stress-rate. The instantaneous moduli in (2.2) are assumed to satisfy the indicial symmetries

$$L_{ijkl} = L_{jikl} = L_{ijlk} = L_{klij}. \tag{2.3}$$

For an elastic–plastic solid the plastic loading moduli, as opposed to the elastic unloading moduli, are pertinent in the bifurcation analysis[5] and these are understood to enter in (2.2).

Three constitutive models which will be used in the study are now given.

J_2 flow theory

Using the x_i-axes as reference, let σ_{ij} be the Cauchy (true) stress, s_{ij} be the deviator stress and $\sigma_e = \sqrt{(3s_{ij}s_{ij}/2)}$ be the effective stress. Then,

$$L_{ijkl} = \frac{2}{3}EI_{ijkl} - (E - E_t)s_{ij}s_{kl}\sigma_e^{-2} \tag{2.4}$$

where E is Young's modulus, E_t is the tangent modulus of the uniaxial true stress–logarithmic strain at σ_e, and

$$I_{ijkl} = \frac{1}{2}(\delta_{ik}\delta_{jl} + \delta_{il}\delta_{jk}) - \frac{1}{3}\delta_{ij}\delta_{kl}. \tag{2.5}$$

J_2 deformation theory

Two versions of a finite strain deformation theory of plasticity will be used. One is a true hyperelastic non-linear elasticity and the other is a hypoelastic (path-dependent) relation. When the principal axes of strain do not rotate relative to the material, both versions coincide and relate the principal components of strain and stress deviator by

$$\epsilon_i = \frac{3}{2}\frac{1}{E_s} s_i \quad (i = 1, 3) \tag{2.6}$$

where E_s is the secant modulus of the uniaxial true stress–logarithmic strain curve at σ_e. In the non-linear elastic version of J_2 deformation theory[6], the material is taken to be isotropic and incompressible with (2.6) as the defining relation between principal strains and stresses whether or not the principal axes of strain rotate with respect to the material. This completely specifies the material. With the aid of Hill's[7] general formulas for the instantaneous shearing moduli of non-linear isotropic elastic solids, one can show that in the principal x_i-axes of the fundamental state

$$L_{ijkl} = \frac{2}{3} E_s I_{ijkl} - (E_s - E_t) s_{ij} s_{kl} \sigma_e^{-2} + Q_{ijkl}. \tag{2.7}$$

The last term in (2.7) shares the indicial symmetries of (2.3); only its "shearing" components are non-zero in principal axes. These are

$$\begin{aligned} Q_{1212} &= \frac{1}{3} E_s[(\epsilon_1 - \epsilon_2)\coth(\epsilon_1 - \epsilon_2) - 1] \\ Q_{1313} &= \frac{1}{3} E_s[(\epsilon_1 - \epsilon_3)\coth(\epsilon_1 - \epsilon_3) - 1] \\ Q_{2323} &= \frac{1}{3} E_s[(\epsilon_2 - \epsilon_3)\coth(\epsilon_2 - \epsilon_3) - 1] \end{aligned} \tag{2.8}$$

where coth is the hyperbolic cotangent.

The Stören–Rice[8] version of J_2 deformation theory does not include Q in (2.7). That is, they take

$$L_{ijkl} = \frac{2}{3} E_s I_{ijkl} - (E_s - E_t) s_{ij} s_{kl} \sigma_e^{-2} \tag{2.9}$$

which leads to path-dependence when the principal axes of strain rotate relative to the material and (2.9) is therefore hypoelastic. Since Q_{1212}, Q_{1313} and Q_{2323} in (2.8) are inherently non-negative, the instantaneous shearing moduli L_{1212}, etc. in (2.7) are generally larger (and never smaller) than their counterparts in (2.9).

All three of the above relations give rise to the same fundamental solution for the stresses under the proportional straining history (2.1)

$$\begin{aligned} \sigma_1 &= 0, \\ \sigma_2 &= \frac{2}{3} E_s(2\cos\alpha + \sin\alpha)X, \\ \sigma_3 &= \frac{2}{3} E_s(\cos\alpha + 2\sin\alpha)X \end{aligned} \tag{2.10}$$

where

$$\sigma_e/E_s = (2/\sqrt{3})X\left(1 + \frac{1}{2}\sin 2\alpha\right)^{1/2}. \tag{2.11}$$

The bifurcation analysis is given in the Appendix. In this section the results of that analysis are summarized and illustrated. At the traction-free surface the velocity components (i.e. displacement increments) of the eigenmode are

$$\begin{aligned} v_1 &= v_1^0 \cos(k_2 x_2)\cos(k_3 x_3) \\ v_2 &= v_2^0 \sin(k_2 x_2)\cos(k_3 x_3) \\ v_3 &= v_3^0 \cos(k_2 x_2)\sin(k_3 x_3) \end{aligned} \tag{2.12}$$

where k_2 and k_3 are wavenumbers which set the scales of the surface variations. The ratios of the amplitude factors v_i^0, one to another, are fixed in a given mode. The bifurcation condition depends only on the relative proportions of k_2 and k_3 and not on their magnitudes and thus it is convenient to write

$$k_2 = k\cos\Omega \quad \text{and} \quad k_3 = k\sin\Omega \tag{2.13}$$

where k is positive and, without loss in generality, $0 \le \Omega \le \pi/2$. For a given history of straining (2.1), the critical mode corresponds to that value of Ω associated with bifurcation at the lowest value of X. As seen in the Appendix, the characteristic length of the exponential decay of the eigenmode beneath the surface is proportional to k.

An important specialization of the family of modes (2.12) is to either $k_3 = 0$ ($\Omega = 0$) or $k_2 = 0$ ($\Omega = \pi/2$),

corresponding to an incremental plane strain mode (e.g. with $k_3 = 0$, $v_3 = 0$ and the variation of v_1 and v_2 is independent of x_3). The incremental plane strain problem has been treated in considerable detail by Hill and Hutchinson[3] and Young[4]. It will be seen that the critical mode is an incremental plane strain field over a significant portion of the range of α. Furthermore, the bifurcation condition can be expressed in closed form for these cases. We now give the results for the incremental plane strain mode for the case $k_3 = 0$ ($\Omega = 0$); the case $k_2 = 0$ is obtained by a trivial conversion.

For an incremental plane strain deformation in the $x_1 - x_2$ plane, (2.2) specializes to

$$\overset{*}{\sigma}_{11} - \overset{*}{\sigma}_{22} = 2\mu^*(\dot{\epsilon}_{11} - \dot{\epsilon}_{22}),\ \overset{*}{\sigma}_{12} = 2\mu\dot{\epsilon}_{12},\ \dot{\epsilon}_{11} + \dot{\epsilon}_{22} = 0 \tag{2.14}$$

where

$$4\mu^* = L_{1111} + L_{2222} - 2L_{1122},\ \mu = L_{1212}. \tag{2.15}$$

Here the notation of Refs. [3, 4] has been used for the two instantaneous shearing moduli, μ for shearing parallel to the 1–2 axes and μ^* for shearing parallel to axes at 45° to the 1–2 axes. Note also that $4\mu^*$ is the tangent modulus governing a plane strain increment of tension parallel to either of the axes. Bifurcation in the surface mode ($\Omega = 0$) occurs when the following condition is first met (Ref. [3], eqn 6.5; Ref. [4], eqn 5.28)

$$\frac{\sigma_2}{4\mu^*} = 1 + \frac{\sigma_2}{4\mu^*}\sqrt{\left(\frac{2\mu - \sigma_2}{2\mu + \sigma_2}\right)}. \tag{2.16}$$

As already mentioned, the scale of the mode as determined by k_2 is arbitrary.

For a solid characterized by J_2 flow theory (2.4), $\mu = E/3$ is the elastic shear modulus and

$$\mu^* = \frac{1}{3}\left[E - (E - E_t)\left(\cos\alpha + \frac{1}{2}\sin\alpha\right)^2\left(1 + \frac{1}{2}\sin 2\alpha\right)^{-1}\right]. \tag{2.17}$$

For $\alpha \neq 0$ or $\alpha \neq \pi$, (2.16) implies that the bifurcation stress for the incremental plane strain mode is on the order of E and thus essentially unattainable in standard polycrystalline metals. For $\alpha = 0$ or $\alpha = \pi$, $\mu^* = \frac{1}{3}E_t$. When $\mu^* \ll \mu$, (2.16) can be replaced by

$$\sigma_2 \cong 2\sqrt{(2\mu\mu^*)} \tag{2.18}$$

which gives $\sigma_2 \cong (2/3)\sqrt{(2EE_t)}$ for $\alpha = 0$ or $\alpha = \pi$. Even in this case, the bifurcation stress or strain is essentially unattainable unless the hardening level is unusually low.

For the first version of J_2 deformation theory (2.7),

$$\mu^* = \frac{1}{3}\left[E_s - (E_s - E_t)\left(\cos\alpha + \frac{1}{2}\sin\alpha\right)^2\left(1 + \frac{1}{2}\sin 2\alpha\right)^{-1}\right] \tag{2.19}$$

$$\mu = \frac{1}{3}E_s(\epsilon_1 - \epsilon_2)\coth(\epsilon_1 - \epsilon_2). \tag{2.20}$$

Numerical results will be presented for a material characterized by a pure power law in uniaxial tension, i.e.

$$\sigma = K\epsilon^N. \tag{2.21}$$

For this material the bifurcation condition (2.16) can be reduced to the following expression for X

$$\zeta X[1 - e^{-\zeta X}] = 2 - \frac{1}{2}(1 - N)\zeta^2\left(1 + \frac{1}{2}\sin 2\alpha\right)^{-1} \tag{2.22}$$

where $\zeta = 2\cos\alpha + \sin\alpha$. The bifurcation condition for the other possible incremental plane strain mode ($k_2 = 0$ and $\Omega = \pi/2$) is obtained simply by taking $\zeta = \cos\alpha + 2\sin\alpha$ in (2.22).

The modulus μ^* is still given by (2.19) according to the hypoelastic version (2.9) of deformation theory but $\mu = E_s/3$, which is smaller than (2.20). Also for this relation the bifurcation condition (2.16) can be reduced to an expression for X, but here only the condition for plane strain deformations ($\alpha = 0$ or $\alpha = \pi$, $\Omega = 0$) will be given. It is

$$\epsilon_2\left[1 - \left(\frac{1 - 2\epsilon_2}{1 + 2\epsilon_2}\right)^{1/2}\right] = N \tag{2.23}$$

while the corresponding result for the true deformation theory from (2.22) is

$$\epsilon_2[1 - e^{-2\epsilon_2}] = N. \tag{2.24}$$

Curves computed from (2.23) and (2.24) showing the bifurcation strain ϵ_2 in plane strain tension and compression are shown in Fig. 1. (The critical mode *is* the incremental plane strain mode with $\Omega = 0$ when $\alpha = 0$ or $\alpha = \pi$, as will be seen below.) The curve for the hypoelastic material terminates at $\epsilon_2 = 1/2$ and $N = 1/2$ since the material ceases to be elliptic at larger strains. Surface bifurcations precede the onset of shear band formation in the hypoelastic material only when $N < 1/2$ in plane strain tension. For the true deformation theory, surface bifurcations precede the onset of shear bands over the entire range of N considered here in plane strain, as will be discussed further below.

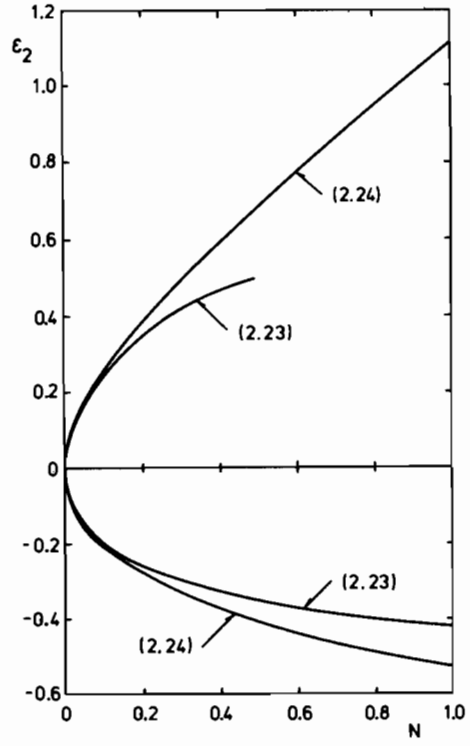

FIG. 1. Bifurcation strain in plane strain tension or compression as function of hardening index N. Curve from true deformation theory is from (2.24) and curve for hypoelastic version is from (2.23).

In the remainder of this section we present numerical results for the true deformation theory (2.7) which deforms in uniaxial tension according to (2.21). The analysis on which the numerical results are based is given in the Appendix. The lowest bifurcation strain for any α can be obtained for $N = 0{\cdot}1$ from Fig. 2 and for $N = 0{\cdot}5$ from Fig. 3. Proportional straining, with α fixed in (2.1), corresponds to progressing along a radial line in Figs. 2 and 3 making an angle α with the ϵ_2-axis, where X is the distance from the origin. For a

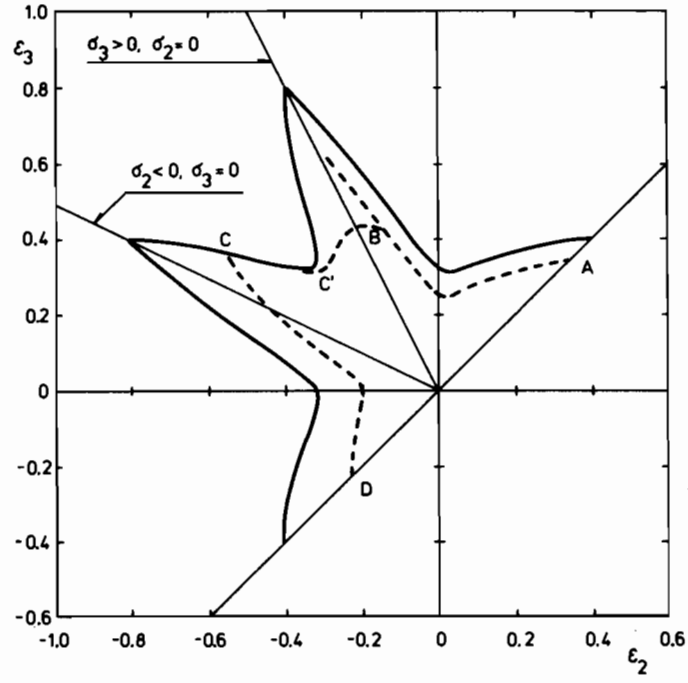

FIG. 2. Critical strains for surface bifurcations for $N = 0{\cdot}1$. Outer curve marks onset of shear bands.

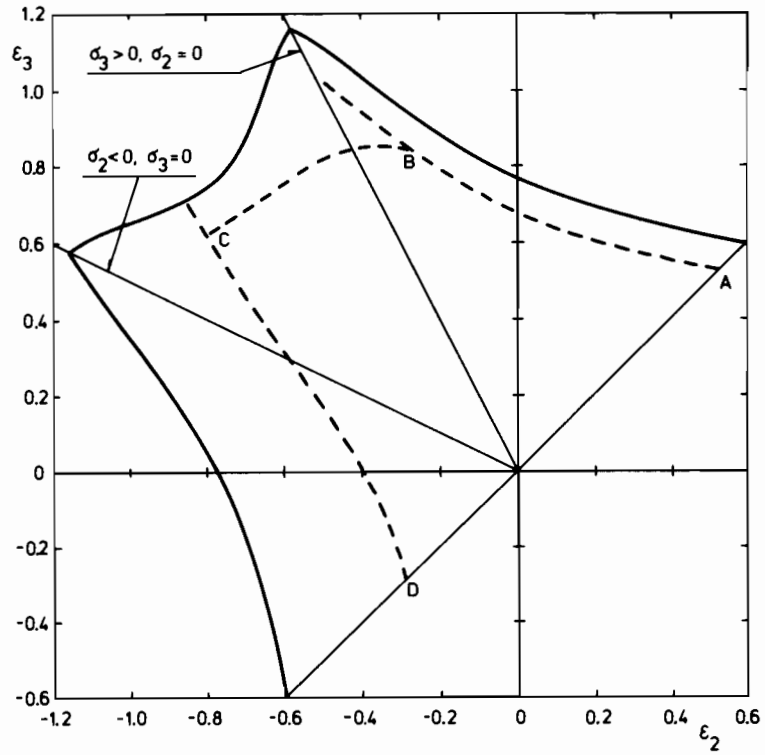

FIG. 3. Critical strains for surface bifurcations for $N = 0{\cdot}5$. Outer curve marks onset of shear bands.

given α, bifurcation first occurs at the strains where the inner curve is intersected. The curves are symmetric about a 45° line through the origin and thus only one half of the figure is shown. Similar plots are used to represent limit strains in sheet metal forming, where they are called forming limit diagrams. In fact, the shapes of the surface bifurcation curves in Figs. 2 and 3 are remarkably similar to the shapes of the forming limit curves in the relevant range where both principal stresses are positive (i.e. $-26{\cdot}6° \leq \alpha \leq 116{\cdot}6°$).

The outer curve in each figure shows the limit of the elliptic region for the material. Outside that curve localized deformation in shear bands becomes possible, as will be discussed further below.

Along the dashed segment AB in Figs. 2 and 3 the critical surface mode is the incremental plane strain mode with $\Omega = 0$ given by (2.22). Along CD the critical mode is the other incremental plane strain mode with deformation increments confined to the x_1–x_3 plane ($\Omega = \pi/2$). On the segment BC the critical mode is not an incremental plane strain field but corresponds to some Ω in the open range $0 < \Omega < \pi/2$. In Fig. 3 for $N = {\cdot}5$, Ω varied monotonically on the branch BC from $\Omega \cong 50°$ at B to $\Omega \cong 26°$ at C. In Fig. 2 for $N = {\cdot}1$, Ω varied from about 55° at B to 35° at C'. On the segment $C'C$ between $\alpha \cong 136°$ and $\alpha \cong 147°$, surface bifurcations did not occur within 99% of the value of X associated with the ellipticity limit.

States A and D, corresponding to equibiaxial tension and compression, respectively, are special in that the bifurcation condition is simultaneously satisfied for both incremental plane strain modes, $\Omega = 0$ and $\Omega = \pi/2$. In fact, all modes, $0 \leq \Omega \leq \pi/2$, are simultaneously available in these states, as has been shown by Bassani, *et al.*[9].

States of uniaxial tension in the 3-direction lie along the radial line $\alpha = 116{\cdot}6°$ in Figs. 2 and 3, while uniaxial compression in the 2-direction corresponds to the line $\alpha = 153{\cdot}4°$. The critical uniaxial strain for surface instabilities is plotted as a function of N in Fig. 4. In tension, ($\sigma_3 > 0$, $\sigma_2 = 0$) the critical mode has $\Omega \cong 47°$ for $N \to 0$ and Ω decreasing monotonically to 29° for $N = 1$. In compression ($\sigma_2 < 0$, $\sigma_3 = 0$) the critical mode is an incremental plane strain mode with $\Omega = 0$.

As mentioned above, the outer curve in Figs. 2 and 3 marks the point in a proportional straining history where shear bands may first emerge. A more extensive study of the onset of shear bands in the J_2 deformation theory solid (2·7) will be presented elsewhere. Here we note without proof that, for the examples in Figs. 2 and 3, the condition for the onset of shear bands is

$$\Delta\epsilon^2 = 4\left[1 - \frac{3}{4}(1-N)\left(\frac{\Delta\sigma}{\sigma_e}\right)^2\right]\left[(\Delta\epsilon \coth \Delta\epsilon - 1) + \frac{3}{4}(1-N)\left(\frac{\Delta\sigma}{\sigma_e}\right)^2\right] \tag{2.25}$$

where $\Delta\sigma$ is the maximum principal stress difference and $\Delta\epsilon$ is the maximum principal strain difference. The shear bands occur on a plane whose normal and shearing direction lie in the plane of the maximum principal stress difference.

3. NON-LINEAR GROWTH OF INITIAL SURFACE IMPERFECTIONS IN PLANE STRAIN

In this section a numerical analysis of the plane strain growth of a small initial surface irregularity is carried out. Prior to any straining the material of the half-space is homogeneous but the traction-free

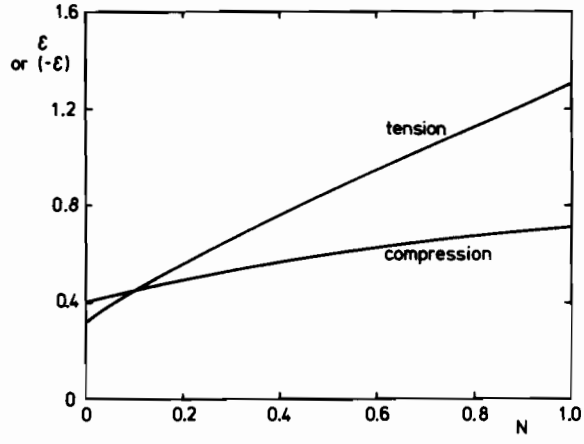

FIG. 4. Critical uniaxial strain for surface bifurcations in uniaxial tension or compression parallel to surface.

surface is displaced vertically from the plane $x_1 = 0$ by

$$h = \frac{1}{2}\delta_0 \cos(\pi x_2/l_0) \tag{3.1}$$

as shown in Fig. 5. The initial half-wavelength of the imperfection l_0 sets the scale of the subsequent deformation. For calculation purposes we choose a cell extending from crest to trough as shown in Fig. 5. The initial width and average depth of the cell are l_0 and a_0. The aspect ratio a_0/l_0 is taken to be sufficiently large such that the non-uniform deformation is confined to the upper portion of the cell, mimicking the infinitely deep half-space.

A Lagrangian formulation of finite strain theory is used with the Cartesian axes x_α ($\alpha = 1,2$) as reference. Displacements, $u_\alpha(x_1, x_2)$ and $u_3 \equiv 0$, of material points are measured from their positions in the undeformed body and the Lagrangian strain tensor is

$$\eta_{\alpha\beta} = \frac{1}{2}(u_{\alpha,\beta} + u_{\beta,\alpha}) + \frac{1}{2}u_{\mu,\alpha}u_{\mu,\beta}. \tag{3.2}$$

Along the bottom of the cell we impose displacement increments such that the vertical displacement remains zero and the horizontal displacement is a uniform stretch, i.e.

$$u_1 = 0 \quad \text{and} \quad u_2 = \left(\frac{l - l_0}{l_0}\right)x_2 \quad \text{on} \quad x_1 = -a_0. \tag{3.3}$$

Thus, l is the deformed width of the cell, and increments of l (or of l/l_0 in a non-dimensional formulation) are prescribed in the calculations. The upper surface of the cell is traction-free, while the lateral faces are free of shearing tractions by symmetry. On the lateral faces,

$$u_2 = 0 \quad \text{and} \quad T_1 = 0 \quad \text{on} \quad x_2 = 0 \tag{3.4}$$

$$u_2 = l - l_0 \quad \text{and} \quad T_1 = 0 \quad \text{on} \quad x_2 = l_0 \tag{3.5}$$

where T_α is the nominal traction vector referred to the x_α axes.

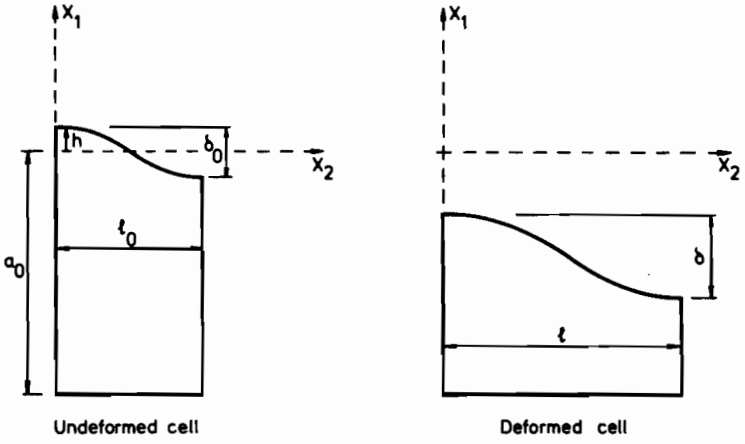

FIG. 5. Schematic views of cell used in numerical calculations.

The numerical solution is obtained by a linear incremental method[10–13] based on finite element solutions of the variational equilibrium equation

$$\int_A \{\dot{\tau}^{\alpha\beta}\delta\eta_{\alpha\beta} + \tau^{\alpha\beta}\dot{u}_{\mu,\alpha}\delta u_{\mu,\beta}\}\,dA = 0 \tag{3.6}$$

where $\tau^{\alpha\beta}$ are the contravariant components of the Kirchhoff stress referred to the deformed base vectors and $\dot{\tau}^{\alpha\beta}$ are the increments of those components. The finite element grid consists of quadrilaterals, each built up from four triangular elements with linear displacement fields. The grid size is varied continuously in the x_1-direction so that the elements are smallest near the surface. A grid of 8×20 quadrilaterials was used in most computations.

Calculations were performed for two constitutive laws; J_2 flow theory and J_2 corner theory.

J_2 flow theory calculations

The formulation for finite strain J_2 flow theory has been described and used elsewhere[10–13] and thus only a curtailed description need be given here. The material is characterized by isotropic hardening based on the J_2 (or σ_e) invariant. For an incompressible material the incremental constitutive law is (2.4) with an appended elastic unloading branch. Conversion of the stresses and moduli to their appropriate components in the deformed base vector system has been described previously[10–13].

To avoid the numerical difficulties associated with plane strain calculations for incompressible materials, we have employed an elastically compressible material with a Poisson's ratio $\nu = 1/3$ in all calculation. It is expected that the numerical results will be essentially identical to those for an incompressible material in the large plastic strain range in which the present phenomena occur. The true stress-logarithmic strain curve of the material in uniaxial tension is taken as

$$\left.\begin{aligned} \sigma/\sigma_0 &= \epsilon/\epsilon_0 \qquad \epsilon \le \epsilon_0 \\ \sigma/\sigma_0 &= (\epsilon/\epsilon_0)^N \qquad \epsilon > \epsilon_0 \end{aligned}\right\} \tag{3.7}$$

where $\sigma_0 = E\epsilon_0$.

It was noted earlier that bifurcation strains were exceptionally large for a solid characterized by J_2 flow theory. It is therefore of interest to see if the non-linear growth of the initial surface waviness can result in significant surface undulations as the solid is strained. The example in Fig. 6 is for a material with $N = 0.1$ and $\epsilon_0 = \sigma_0/E = 0{\cdot}005$ and for an initial waveheight to half-wavelength ratio $\delta_0/l_0 = 0{\cdot}004$. The upper plot shows the history of δ/l_0 as a function of the overall imposed strain

$$\epsilon_a = \ln(l/l_0). \tag{3.8}$$

The lower plot shows the ratio of the maximum principal strain component $\epsilon_{max} = \epsilon_2$ at the bottom of the trough on the surface to ϵ_a. Calculations were made using a mesh with 8×40 quadrilaterals for $a_0/l_0 = 20$ since the decay length for the flow theory is large compared to l. Fig. 6 shows rather little growth of the initial waviness and of the maximum strain at least for overall strains less than about unity. The early behaviour is essentially the same as for the J_2 corner theory discussed below.

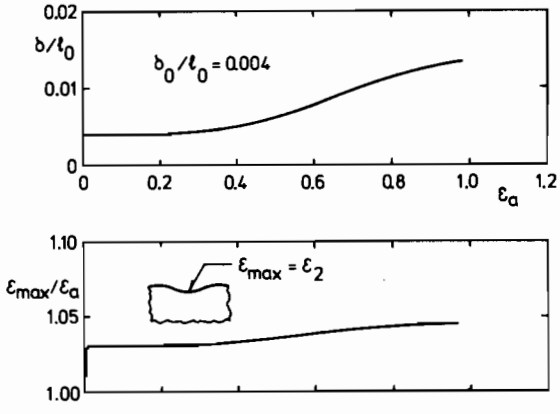

FIG. 6. Growth of initial waviness as function of overall tensile strain ϵ_a for J_2 flow theory with $\epsilon_0 = 0{\cdot}005$ and $N = 0{\cdot}1$.

J_2 corner theory calculations

The instantaneous moduli from a deformation theory model the instantaneous moduli of an elastic–plastic solid which develops a corner, or vertex, at the loading point on the yield surface when the stress increments are nearly proportional. Bifurcations in an elastic–plastic solid characterized by a corner does take place in such a way that nearly proportional stressing occurs everywhere[5], and this is the justification for use of deformation theory moduli in bifurcation calculations for elastic–plastic solids. But deformation theory cannot continue to represent an elastic–plastic solid in the post-bifurcation response in most applications, including the present, since strong deviations from proportional stressing almost always occur.

Recently, a phenomenological corner theory of plasticity, called J_2 corner theory, was proposed by Christoffersen and Hutchinson[14]. That theory is constructed such that the instantaneous moduli coincide with those of J_2 deformation theory (in either form) for nearly proportional loading increments and increase smoothly until they coincide with the elastic moduli for stress increments directed along or within the corner of the yield surface. Thus the bifurcation predictions from J_2 corner theory are precisely the same as those from the corresponding version of J_2 deformation theory.

Let $\mathbf{L}^0$ denote the instantaneous moduli from either version of the J_2 deformation theory, (2.7) or (2.9), but including elastic compressibility so that $\overset{*}{\sigma}_{ij} = L^0_{ijkl}\dot{\epsilon}_{kl}$. Let the compliances $\mathbf{M}^0$ be the inverse of $\mathbf{L}^0$ and let $\mathcal{M}$ be the elastic compliances. The "plastic part" of the strain-rate from deformation theory is

$$\dot{\epsilon}^p_{ij} = C_{ijkl}\overset{*}{\sigma}_{kl} \text{ where } C_{ijkl} = M^0_{ijkl} - \mathcal{M}_{ijkl}. \tag{3.9}$$

Thus, $\mathbf{C}$ is the instantaneous plastic compliance tensor from deformation theory. In J_2 corner theory the yield surface in the neighborhood of the loading point is a cone in stress-space with axis

$$\lambda_{ij} = s_{ij}(C_{mnpq}s_{mn}s_{pq})^{-1/2} \tag{3.10}$$

where s_{ij} is the current stress deviator. The positive angular measure θ of the stress-rate from the cone axis, and thus from proportional loading, is defined by

$$\cos\theta = C_{ijkl}\lambda_{ij}\overset{*}{s}_{kl}(C_{mnpq}\overset{*}{s}_{mn}\overset{*}{s}_{pq})^{-1/2}. \tag{3.11}$$

A stress-rate potential is defined by

$$W = \frac{1}{2}\mathcal{M}_{ijkl}\overset{*}{\sigma}_{ij}\overset{*}{\sigma}_{kl} + \frac{1}{2}f(\theta)C_{ijkl}\overset{*}{\sigma}_{ij}\overset{*}{\sigma}_{kl} \tag{3.12}$$

and the total strain-rate is obtained from it by

$$\dot{\epsilon}_{ij} = \partial W/\partial\overset{*}{\sigma}_{ij} = (\partial^2 W/\partial\overset{*}{\sigma}_{ij}\partial\overset{*}{\sigma}_{kl})\overset{*}{\delta}_{kl}. \tag{3.13}$$

This leads to incremental compliances and moduli which depend on θ, i.e.

$$\dot{\epsilon}_{ij} = M_{ijkl}(\theta)\overset{*}{\sigma}_{kl} \tag{3.14}$$

and

$$\overset{*}{\sigma}_{ij} = L_{ijkl}(\theta)\dot{\epsilon}_{kl} \tag{3.15}$$

where $\mathbf{L}$ is the inverse of $\mathbf{M}$.

With θ_c as the cone angle in stress-rate space, elastic unloading occurs for $\theta_c \le \theta \le \pi$ and $f(\theta) = 0$. The total loading range is specified by $\theta \le \theta_0$ with $f(\theta)1$ so that within this range corner theory coincides with deformation theory. In other words, $\mathbf{L}$ is the tensor of deformation theory moduli for $\theta \le \theta_0$ and $\mathbf{L}$ is the tensor of elastic unloading moduli for $\theta_c \le \theta \le \pi$. In the transition region, $\theta_0 \le \theta \le \theta_c$, $f(\theta)$ is chosen to smoothly merge the deformation theory moduli with the elastic moduli in a way which ensures convexity of the incremental relation. Further details, including the specification of $f(\theta)$, are given in the Appendix, along with a brief discussion of implementation of the theory in the finite element scheme.

The numerical results shown in Figs. 7 and 8 were obtained using the corner theory based on the true deformation theory moduli (2.7). The theory was fit to the same tensile stress–strain curve (3.7) used for the J_2 flow theory calculations with $\epsilon_0 = 0{\cdot}005$ and $\nu = 1/3$. Here the aspect ratio $a_0/l_0 = 4$ was sufficiently large to eliminate interaction of the free surface and the bottom of the cell. For plane strain tension in Fig. 7 with $N = 0{\cdot}1$, the bifurcation strain of the perfect half-space is $\epsilon_a = 0{\cdot}25$, while in Fig. 8 for compression it is $\epsilon_a = -0{\cdot}20$. Shown is the growth of δ/l_0 and $\epsilon_{max} = \epsilon_2$ at the bottom of the trough normalized by ϵ_a in (3.8) for two levels of initial waviness, $\delta_0/l_0 = 0{\cdot}0004$ and $0{\cdot}004$. For the smaller imperfection the waveheight grows relatively little until the overall strain is approximately the bifurcation strain of the perfect half-space and then it grows rapidly with increasing overall strain. In the case of the larger imperfection the waves show noticeable amplification at lower levels of overall straining.

Fig. 9 displays a comparison of predictions from the two versions of the corner theory, one based on (2.7) and the other on (2.9), for $N = 0{\cdot}2$ and $\delta_0/l_0 = 0{\cdot}0004$ in plane strain tension. The respective bifurcation strains for the perfect case are $\epsilon_a = 0{\cdot}38$ and $0{\cdot}35$. The curves are shifted by an amount which is approximately equal to the difference between the bifurcation strains and are otherwise similar. In each case the stressing is essentially proportional (except in the very early stages when the elastic and plastic strains are of comparable magnitude) until the overall strain attains the respective bifurcation strain. Complete elastic unloading (i.e. $\theta > \theta_c$) is not observed at any point in the body even after the upturn in the growth of the surface wave. However a region in which the material response has entered the "non-linear" range $\theta_0 \le \theta \le \theta_c$ starts pointwise when the overall strain is about the bifurcation strain and spreads into the body.

In summary, it appears that a solid characterized by a smooth yield surface and isotropic hardening is not susceptible to surface instabilities within the range of strains investigated here, while a solid modelled by a yield surface which develops a corner is susceptible. To an extent the situation is parallel to that of necking in thin sheets under biaxial tensile stretching. A thin sheet characterized by deformation theory does undergo bifurcations at strains which are in at least qualitative agreement with experiments[8]. A perfect sheet of material characterized by J_2 flow theory does not undergo necking bifurcations when both

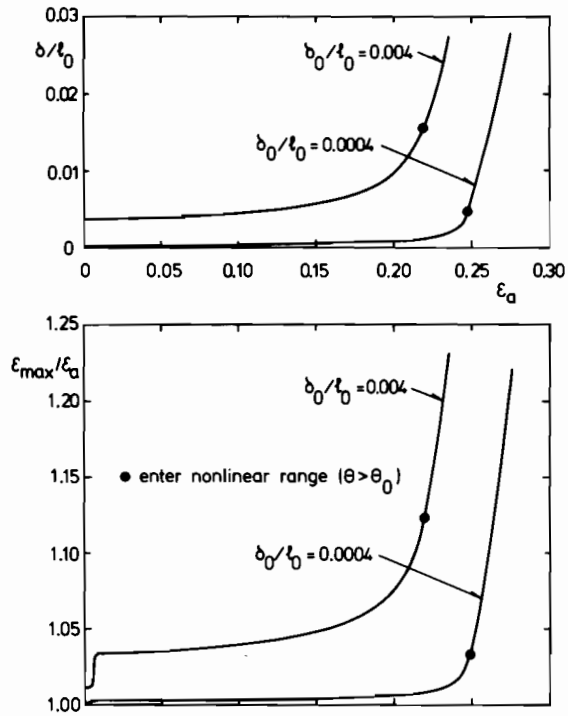

FIG. 7. Growth of initial waviness as function of overall tensile strain ϵ_a for J_2 corner theory with $\epsilon_0 = 0{\cdot}005$ and $N = 0{\cdot}1$.

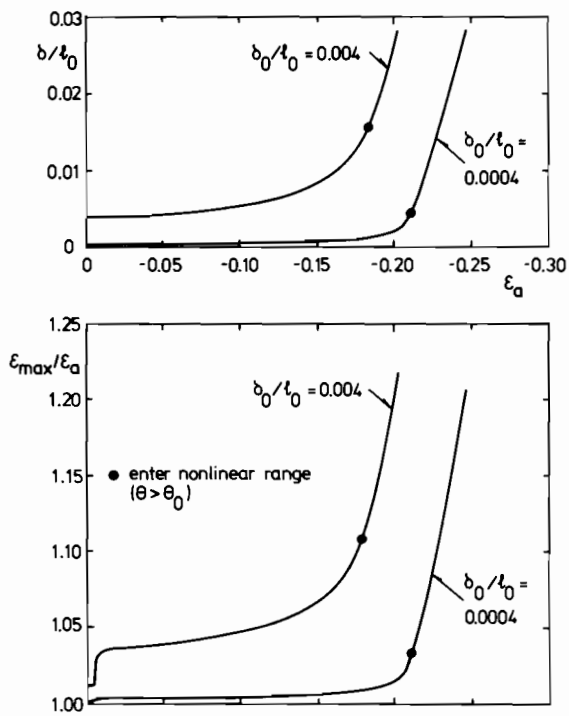

FIG. 8. Growth of initial waviness as function of overall compressive strain ϵ_a for J_2 corner theory with $\epsilon_0 = 0{\cdot}005$ and $N = 0{\cdot}1$.

principal in-plane strains are tensile. However, a non-linear growth analysis of an initially imperfect sheet *does* predict necking when J_2 flow theory is used, although at strains which are substantially larger than those observed experimentally. The same non-linear growth analysis using a kinematic hardening characterization of the yield surface predicts overall necking strains which are reasonably close to the deformation theory predictions[15]. The high curvature of the kinematic hardening yield surface of a hardening material at moderately large strains, by comparison to the low curvature of the isotropic hardening surface,

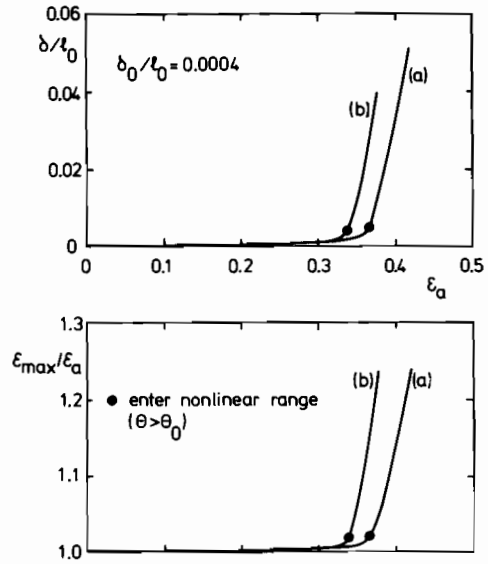

FIG. 9. Comparison of predictions for two versions of corner theory based on (a) the true deformation theory and (b) the hypoelastic deformation theory. In both cases $\epsilon_0 = 0{\cdot}005$ and $N = 0{\cdot}2$.

is not far removed from a corner. It would be of considerable interest to repeat the analysis of Fig. 6 using kinematic hardening theory and thus to determine whether surface instabilities are only associated with cornered yield surfaces. As in other necking-like phenomena, one expects material rate-dependence to have a very strong influence on the growth of surface waves.

4. OBSERVATIONS OF SURFACE INSTABILITIES

A few bend tests have been made in the laboratory to observe surface roughness that develops on aluminum bars. The surfaces of the bar are in a state of either plane strain tension or compression away from the edges, to a good approximation. The gradient of strain through the bar limits the wavelength of any surface mode to be small compared to the thickness.

The commercial aluminum bar used for these experiments has the cross-sectional dimensions 40×15 mm. In a uniaxial tensile test Young's modulus and the yield stress for this material are found as $E = 66000$ MPa and $\sigma_0/E = 0{\cdot}0038$ and the response can be approximated as power hardening with $N \cong 0{\cdot}04$. The average grain diameter inside the bar is approximately 70–100 μm. At the surface one or two layers of grains are larger, with dimensions around 350–400 μm in the longitudinal direction, 140–170 μm along the width and 70–100 μm in the normal direction.

The tests are made both for the original surface of the bar and for a bar with 1 mm material machined off the surface, so that the new surface has the small grain size characteristic of the inside of the bar. Machining is made in the longitudinal direction of the bar so that the machining traces will not interact with the surface waves predicted by the theory. In the tests it is quite clear that a larger grain size gives more roughness (i.e. larger δ but not necessarily larger δ/l) and that the roughness increases with increasing strain, as has been observed by previous authors (e.g. Kienzle[16]). The point of main interest in the present investigation is however not as much the grainy appearance of the deformed surface as the tendency to form waves perpendicular to the principal direction of stretching or compression.

The stretched surface shown in Fig. 10(a) is the original surface of the bar, whereas in Fig. 10(b) 1 mm of material has been machined off; in each case the surface has experienced an overall strain level of about 0·3–0·5. In both cases there is a pattern corresponding to grain size, but the main wavelength in Fig. 10(a) is about 2–3 grain sizes and in Fig. 10(b) about 6–8 grain sizes superposed on the fine pattern. The orientation of the waves is that of the predicted incremental plane strain mode. Fig. 10(c) shows the original surface stretched somewhat further than in Fig. 10(a). It is seen that the large strains at the very bottom of the wave troughs lead to shear fracture that propagates deep into the bar.

Hahn and Rosenfield[17] have observed surface irregularities in plane strain tension which they label as superbands. These bands run perpendicular to the maximum tensile direction and are about one grain in width and many grains long. Micro-cracks were observed to develop at the bottom of the bands and to grow into a shear fracture running along the band, similar to what is seen in Fig. 10(c).

The wavelength to be expected in the present tests is set by the initial imperfections present in the bar, assuming they are very small compared to the thickness. Wavelengths comparable with a few grain sizes seem natural, as the major effective imperfection is probably represented by the grains. On the compressive side the patterns were similar but not quite as distinct, particularly in the case of original large grained surface. Wrinkles on the compression side of bent bars have also been observed[18, 19] for steel specimens.

A very nice wave pattern appeared on some specimens of Larsson[20] during an experimental investigation of the instability of closed-ended thick-walled cylinders under internal pressure. Here the axisymmetric state of deformation bifurcates into an eccentric shape and during the final collapse the tube bulges out in one region with considerable extra straining until fracture occurs. The state of deformation is again approximately plane strain tension in the circumferential direction, at least before substantial bulging occurs. Fig. 11 shows that surface waves parallel with the tube axis have developed in the highly strained

region, where final fracture has occurred. The waves with a wavelength of about 0·25 mm appear only in the highly strained region and are clearly perpendicular to the direction of machining and in the direction predicted by the theory. The tube of Fig. 11 is one of a number of aluminum specimens on which waves appeared in all cases, whereas no waves were observed on a similar series of copper specimens[20]. The aluminum alloy employed has a strain hardening exponent $N \cong 0{\cdot}1$ and the copper has $N \cong 0{\cdot}33$.

Initial surface roughness develops as a consequence of heterogoneous deformation at the scale of the crystalline grains. We speculate that, once the critical conditions have been met for surface instabilities to grow, the roughness tends to become more correlated, consistent with the critical surface mode, and begins to develop more rapidly. There is some evidence that surface roughness on thin sheets under biaxial straining does start to grow rather dramatically (outside the neck region) after an initial period of relatively slow development[21].

REFERENCES

1. M. A. BIOT, *Mechanics of Incremental Deformation*. Wiley, New York (1965).
2. K. N. SAWYERS, In *Finite Elasticity, AMD*, Vol. 27, (Edited by R. S. Rivlin) *ASME*, New York (1977).
3. R. HILL and J. W. HUTCHINSON, *J. Mech. Phys. Solids* **23**, 239 (1975).
4. N. J. B. YOUNG, *J. Mech. Phys. Solids* **24**, 77 (1976).
5. R. HILL, In *Problems of continuum mechanics* **155**, *S. I. A. M.* Philadelphia (1961).
6. J. W. HUTCHINSON and K. W. NEALE, In *Mechanics of sheet metal forming*. Vol. 127. Plenum, New York (1978).
7. R. HILL, *Proc. Roy. Soc. London A*, **314**, 457 (1970).
8. S. STÖREN and J. R. RICE, *J. Mech. Phys. Solids* **23**, 421 (1975).
9. J. L. BASSANI, D. DURBAN and J. W. HUTCHINSON, *Math. Proc. Camb. Phil. Soc.* **87**, 339 (1980).
10. J. W. HUTCHINSON, In *Numerical solution of non-linear structural problems* (Edited by R. F. Hartung), AMD-Vol. 17, *ASME*, New York (1973).
11. R. M. MCMEEKING and J. R. RICE, *Int. J. Solids Struct.* **11**, 601 (1975).
12. A. NEEDLEMAN, *J. Appl. Mech.* **39**, 964 (1972).
13. V. TVERGAARD, Influence of voids on shear band instabilities under plane strain conditions, Danish Center for *Appl. Math.* and *Mech.*, Rep. No. 159 (1979).
14. J. CHRISTOFFERSEN and J. W. HUTCHINSON, *J. Mech. Phys. Solids* **27**, 465 (1979).
15. V. TVERGAARD, *Int. J. Mech. Sci.* **20**, 651 (1978).
16. O. KIENZLE, *Werkstoffstechnik* **56**, 542 (1966).
17. G. T. HAHN and A. R. ROSENFIELD, *Met. Trans. A.* **6A**, 653 (1975).
18. D. C. DRUCKER, private communication, refers to work with Ludley and Myloans.
19. R. H. HAWLEY and D. C. DRUCKER, *Experimental Mechanics* **13**, 1 (1973).
20. M. LARSSON, Instabilities in closed-end thickwalled cylinders subject to internal pressure, Thesis for Diploma, Dept. of Strength of Materials and Solid Mechanics, The Royal Institute of Technology, Stockholm (in Swedish) (1978).
21. G. R. BARBA and G. L. FERRAN, Evolucao da rugosidade superficial de chapa de aco durante a conformacão *Metalurgia ABM* (To be published (1979)).

Acknowledgements—The authors thank Prof. B. Storåkers of Stockholm for making available one of M. Larsson's specimens shown in Fig. 11. The work was initiated while one of us (J.W.H.) was visiting at and supported by the Solid Mechanics Department of the Technical University of Denmark. The later stages of the work by J.W.H. were supported in part by the U.S. National Science Foundation under Grant NSF-ENG78-10756 and by the Division of Applied Sciences, Harvard University.

APPENDIX

Bifurcation analysis

In the x_i-axes introduced in Section 2 with (2.2) specifying the incremental relation, the non-zero moduli are L_{1111}, L_{2222}, L_{3333}, L_{1122}, L_{1133}, L_{2233}, L_{1212}, L_{1313} and L_{2323} together with the components related to these by the indicial symmetries (2.3). Equilibrium requires

$$\dot{n}_{ij,i} = 0 \quad (j = 1,3) \tag{A1}$$

where $\dot{n}_{ij}$ is the nominal stress-rate. Using the relation between the Jaumann-rate of Cauchy stress and the nominal stress-rate, one can show that (A1) can be rewritten as

$$c_{ijkl} v_{l,ki} + g_{,j} = 0 \quad (v_{p,p} = 0) \tag{A2}$$

for $j = 1,3$ where

$$c_{ijkl} = L_{ijkl} + \frac{1}{2}\sigma_{ik}\delta_{lj} - \frac{1}{2}\sigma_{il}\delta_{kj} - \frac{1}{2}\sigma_{jk}\delta_{li} - \frac{1}{2}\sigma_{jl}\delta_{ki} \tag{A3}$$

Equation (A2) admits solutions of the form

$$\begin{aligned} v_1 &= A_1 e^{zkx_1} \cos(k_2 x_2) \cos(k_3 x_3) \\ v_2 &= A_2 e^{zkx_1} \sin(k_2 x_2) \cos(k_3 x_3) \\ v_3 &= A_3 e^{zkx_1} \cos(k_2 x_2) \sin(k_3 x_3) \\ g &= G e^{zkx_1} \cos(k_2 x_2) \cos(k_3 x_3) \end{aligned} \tag{A4}$$

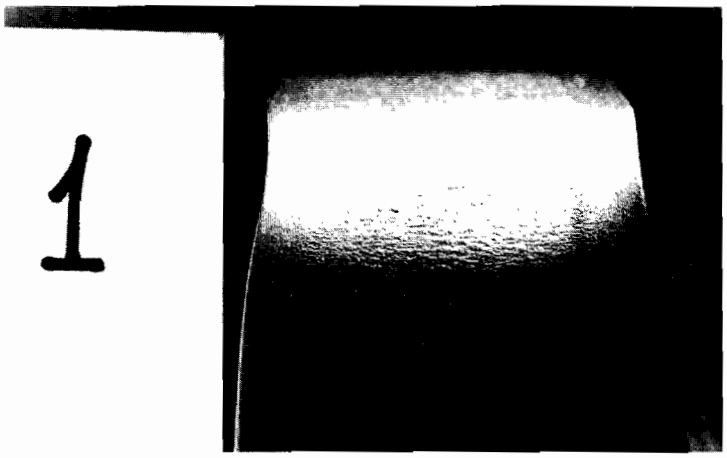

(a)

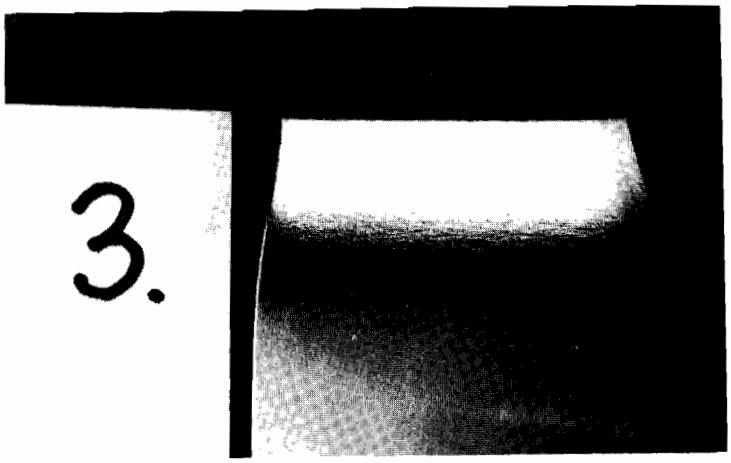

(b)

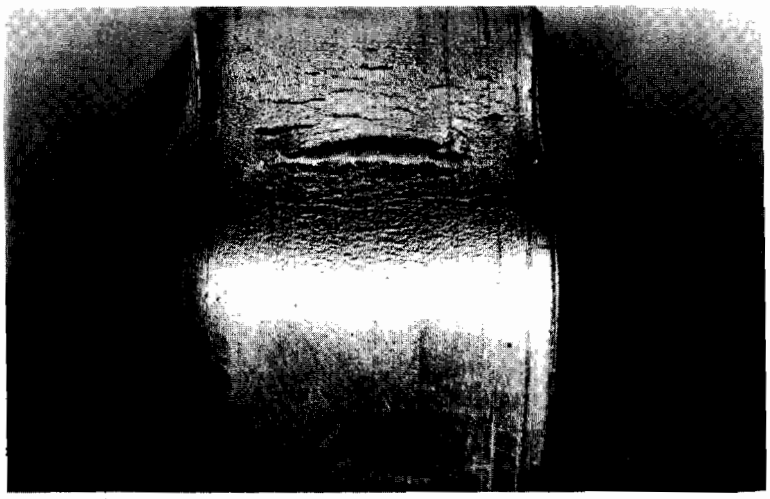

(c)

FIG. 10. Stretched surfaces on bent aluminum bars. (a) Original surfaces. b) Surface obtained by machining off 1 mm material. (c) Original surface stretched to fracture.

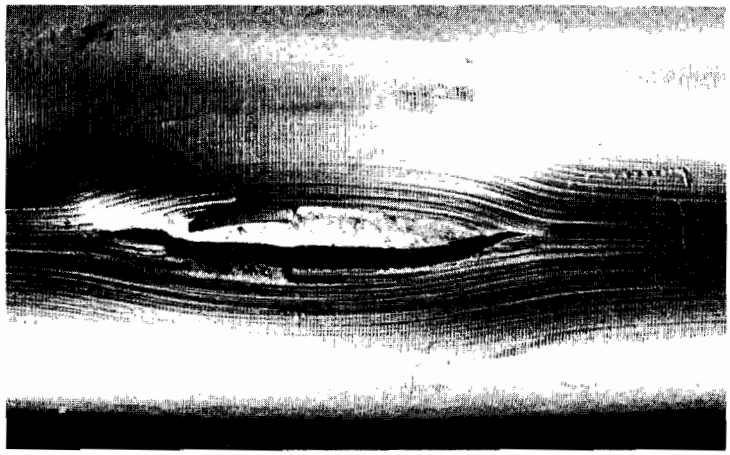

FIG. 11. Surface wave pattern in highly strained region on pressurized aluminum cylinder (Larsson [20]).

where the k's were introduced in (2.12) and (2.13), z may be complex, and the A_i and G may also be complex. Here and below, physical quantities are given by the real part of a complex expression. Incompressibility requires

$$A_1 zk + A_2 k_2 + A_3 k_3 = 0 \tag{A5}$$

Substitution of (A4) into (A2) using (A5) to eliminate A_1 leads to three homogeneous equations for $A_2 k_2$, $A_3 k_3$ and G. The requirement that the determinant of the system of equations vanish gives a cubic equation for z^2, i.e.

$$z^6 + d_1 z^4 + d_2 z^2 + d_3 = 0. \tag{A6}$$

The coefficients d_i are real; they depend on the c_{ijkl} and on Ω but not on k. The expressions for d_i are somewhat lengthy, but easily derived, and will not be listed.

In the elliptic range there are three roots z of (A6) with positive real part; denote them by z_i ($i = 1,3$). At least one of the roots is real. The other two are either real or are complex conjugates of one another, depending on the c_{ijkl} and on Ω.

Let $A_{j(i)}$ ($j = 1,3$) and $G_{(i)}$ be a solution to the homogeneous equations (A2) and (A5) associated with z_i. These are assumed to be normalized in some convenient fashion. The eigenmode is a linear combination of the three solutions (A4) for which z has a positive real part, i.e.

$$v_1 = \sum_{i=1}^{3} \xi_i \mathcal{R}[A_{1(i)} e^{z_i k x_1}] \cos(k_2 x_2) \cos(k_3 x_3)$$

$$g = \sum_{i=1}^{3} \xi_i \mathcal{R}[G_{(i)} e^{z_i k x_1}] \cos(k_2 x_2) \cos(k_3 x_3) \tag{A7}$$

where $\mathcal{R}[\ ]$ denotes the real part and analogous expressions hold for v_2 and v_3. The conditions for zero traction-rate on $x_1 = 0$ are $\dot{n}_{1j} = 0$ ($j = 1,3$) and these reduce to a set of three equations for the ξ_i of the form

$$\sum_{i=1}^{3} H_{ji} \xi_i = 0 \quad (j = 1,3). \tag{A8}$$

The H_{ji} are real and are readily obtained from the previous expressions; they depend implicitly on the current state (i.e. on X and α) and on Ω. The eigenvalue equation for a non-trivial solution to (A8) is the vanishing of the determinant of the 3×3 matrix H_{ji}, assuming no two roots z_i are equal.

An alternative procedure, which is better suited to numerical work, is to evaluate the symmetric matrix S where

$$\int_{-\infty}^{0} dx_1 \int_{-\pi/k_2}^{\pi/k_2} dx_2 \int_{-\pi/k_3}^{\pi/k_3} dx_3 c_{ijkl} v_{j,i} v_{l,k} = \sum_{i=1}^{3} \sum_{j=1}^{3} \xi_i \xi_j S_{ij}.$$

Below the lowest eigenstate, S is positive definite for all Ω. The lowest eigenvalue X is associated with that value of Ω for which S first becomes positive semi-definite, assuming no two roots z_i are equal. For a given α, X was increased in small steps and the positive definiteness of S was checked at many values of Ω over the range $0 < \Omega < \pi/2$. The critical value of X for $\Omega = 0$ or $\pi/2$ is (2.22). An exceptional Ω where two roots are equal does not require special treatment since, if it corresponds to the critical mode, S will lose positive definiteness at slightly higher X for Ω in a range about the exceptional value.

J_2 corner theory

The notation for the corner theory used in Section 3 and below is the same as that employed in Ref. [14] and the reader is referred to that reference for full details of the theory. Here we simply complete the specification of the function $f(\theta)$ in the transition range $\theta_0 \le \theta \le \theta_c$.

In stress-space the yield surface cone in the vicinity of the current deviator stress is specified by $\beta = \beta_c$ where

$$\cos\beta = \dot{\sigma}_e \left(\frac{3}{2} \overset{*}{s}_{ij} \overset{*}{s}_{ij} \right)^{-1/2} \tag{A9}$$

In the present calculations we took

$$\tan\beta_c = -\sigma_0 (\sigma_e^2 - \sigma_0^2)^{-1/2} \quad \text{for} \quad \frac{\pi}{2} \le \beta_c \le \frac{3\pi}{4} \tag{A10}$$

and we limited the cone angle so that it was never sharper than $3\pi/4$. Thus, once the strains were well into the plastic range the cone angle β_c is fixed at $3\pi/4$. The cone angle θ_c in stress-rate space is given by [14]

$$\tan\theta_c = \sqrt{a} \tan\beta_c, \quad a = \left(\frac{E}{E_s q} - 1 \right) \left(\frac{E}{E_t} - 1 \right)^{-1} \tag{A11}$$

where $q = 1$ for the version (2.9) and $q = (\sqrt{3}\sigma_e/E_s) \coth(\sqrt{3}\sigma_e/E_s)$ when (2.7) is used in plane strain with compressibility neglected.

The plastic strain-rate vector falls within the range $0 \le \theta \le \theta_n$ where $\theta_n = \theta_c - \pi/2$. The total loading

range, $0 \le \theta \le \theta_0$, was taken to be $\theta_0 = 1/2\theta_n$. The function $f(\theta)$ is defined by (Ref. [14], Section 2)

$$f(\theta) = \frac{1}{g(\phi)[1 + l^2(\phi)]}, \quad \theta(\phi) = \phi + \arctan(l(\varphi)) \tag{A12}$$

where

$$l(\phi) = \frac{1}{2}(\mathrm{d}g/\mathrm{d}\phi)g^{-1}$$

and

$$g(\phi) = \begin{cases} 1 & 0 \le \phi \le \theta_0 \\ \{1 - [(\phi - \theta_0)/(\theta_n - \theta_0)]^3\}^{-2} & \theta_0 \le \phi \le \theta_n \end{cases}. \tag{A13}$$

The expression for the instantaneous compliances $\mathbf{M}(\theta)$ in (3.14) are given in Ref. [14]; $\mathbf{L}(\theta)$ is obtained as its numerical inverse.

The components of the moduli must be transformed to the deformed base vectors in the same manner as is done in the J_2 flow theory calculation. The direction of the stress-rate as measured by θ should, in principle, be obtained by iteration at each incremental step. However a simpler scheme proved to be accurate in which θ is taken to be the value determined in the previous step. Since small increments are used in the computation anyway, this scheme leads to small errors and appeared to introduce no numerical instabilities.